Title: Human Umbilical Cord blood monocytes, but not adult blood monocytes, rescue brain cells from hypoxic-ischemic injury: Mechanistic and therapeutic implications

Running Title: Cord blood monocytes protect neurons from OGD

Authors: Arjun Saha*, Sachit Patel†, Li Xu, Paula Scotland, Jonathan Schwartzman, Anthony J. Filiano, Joanne Kurtzberg and Andrew E. Balber

Authors' institution: Marcus Center for Cellular Cures (MC3), Duke University School of Medicine, Durham, North Carolina, USA

†current address: Department of Pediatrics, Division of Pediatric Blood and Marrow Transplantation, University of Nebraska Medical Center, Omaha, Nebraska

Author contributions:

Arjun Saha: Conception, experimental design, collection, assembly, analysis and interpretation of data, writing and final approval of manuscript.

Sachit Patel: Collection, assembly, and analysis of data, final approval of manuscript.

Li Xu: Collection, assembly and analysis of data, final approval of manuscript.

Paula Scotland: Collection, assembly and analysis of data, final approval of manuscript

Jonathan Schwartzman: Analysis of data, final approval of manuscript

Anthony Filiano: Analysis of data, reviewing and final approval of manuscript.

Joanne Kurtzberg: Funding acquisition, direction of clinical development program, provision of study materials, data interpretation, writing and final approval of manuscript.

Andrew Balber: Conception and design; analysis of data, writing and final approval of manuscript.

***Corresponding author:** Arjun Saha, PhD, Duke University School of Medicine, Durham, NC 27710. Phone: 919-684-3934. FAX: 919- 681-9760. Email: arjun.saha@duke.edu

Abstract (225/300)

Cord blood (CB) mononuclear cells (MNC) are being tested in clinical trials to treat hypoxic-ischemic (HI) brain injuries. Although early results are encouraging, mechanisms underlying potential clinical benefits are not well understood. To explore these mechanisms further, we exposed mouse brain organotypic slice cultures to oxygen and glucose deprivation (OGD) and then treated the brain slices with cells from CB or adult peripheral blood (PB). We found that CB-MNCs protect neurons from OGD-induced death and reduced both microglial and astrocyte activation. PB-MNC failed to affect either outcome. The protective activities were largely mediated by factors secreted by CB-MNC, as direct cell-to-cell contact between the injured brain slices and CB cells was not essential. To determine if a specific subpopulation of CB-MNC are responsible for these protective activities, we depleted CB-MNC of various cell types and found that only removal of CB $CD14^+$ monocytes abolished neuroprotection. We also used positively selected subpopulations of CB-MNC and PB-MNC in this assay and demonstrated that purified CB-$CD14^+$ cells, but not CB-PB $CD14^+$ cells, efficiently protected neuronal cells from death and reduced glial activation following OGD. Gene expression microarray analysis demonstrated that compared to PB-$CD14^+$ monocytes, CB-$CD14^+$ monocytes over-expressed several secreted proteins with potential to protect neurons. Differential expression of five candidate effector molecules, chitinase 3-like protein-1, inhibin-A, interleukin-10, matrix metalloproteinase-9 and thrombospondin-1, were confirmed by western blotting, and immunofluorescence. These findings suggest that $CD14^+$ monocytes are a critical cell-type when treating HI with CB-MNC.

Key words: Cell therapy, cord blood, hypoxic-ischemic injury, monocyte, oxygen-glucose deprivation.

Abbreviations: CB, cord blood; HI, hypoxia-ischemia; HIE, hypoxic- ischemic encephalopathy; MNC, mononuclear cell; OGD, oxygen glucose deprivation; PB, peripheral blood.

Introduction

Mononuclear cell (MNC) prepared from human umbilical cord blood (CB) are candidate therapeutics for treating hypoxic-ischemic (HI) brain injuries. Patients with cerebral palsy [1-4], neonatal hypoxic-ischemic encephalopathy (HIE) [5], and acute ischemic stroke [6] have been treated with intravenously administered CB-MNC in early safety and feasibility trials. Some signals of efficacy have emerged in a Phase 2 trial in young children with cerebral palsy [7], and additional clinical studies involving treatment of ischemic brain injury with CB are currently listed as open on ClinTrials.gov (stroke, NCT02433509, . NCT0167393, NCT0300497, NCT0143859, NCT02881970; neonatal hypoxic ischemic encephalopathy, NCT0243496, NCT02612155, NCT0225661, NCT0255100, NCT0228707; various conditions, NCT0332746).

Many preclinical studies suggest that CB-MNC protect the brain after HI by releasing neurotrophic and anti-inflammatory factors that stimulate repair by host cells [8, 9]. These studies, using various animal and culture systems, have implicated different CB-MNC subpopulations in contributing to neuroprotection [10-17]. CB-MNC protect primary astrocytes [18], oligodendrocytes [19, 20], and microglia [18], as well as neuronal cell lines [15] from HI-induced injury. However, what factors mediate brain repair, the CB-MNC cell types that contribute, and the host cells with which they interact are unclear. Determining which cell types in CB-MNC enhance brain tissue repair, and the mechanisms by which they do so, will optimize decisions on dosing, route of administration, treatment frequency, and other critical clinical and regulatory parameters. This information may also help in the development of mechanism-based potency assays for advanced clinical testing and, ultimately, for manufacturing and releasing products for clinical use.

In this paper, we present experiments that address these questions using organotypic mouse brain slice cultures exposed to oxygen-glucose deprivation (OGD) [21-24]. The brief OGD exposure triggers a neuro-inflammatory cascade involving activation of microglia and astrocytes that leads to the death of neurons over 2 to 3 days. Because the brain architecture and cell types are preserved in this model, the pathogenic mechanisms induced by OGD in brain slices are similar to those causing HI brain injuries *in vivo* [25]. Thus, this model can be used to test cell therapies for neuroprotection following OGD [19, 25]. We report here that CB-MNC protect neurons from death and dampen the activation of astrocyte and microglia in slice cultures exposed to OGD. This neuroprotection was mediated by $CD14^+$ monocytes in the CB-MNC. Unlike CB monocytes, $CD14^+$ monocytes from adult peripheral blood (PB) did not confer protection to neurons or reduced glial activation. We identified several candidates upregulated, at the RNA and protein levels, in CB monocytes compared to PB monocytes that may play a role in neuroprotection and repair. These findings will inform late stage clinical development of CB-MNC products for treatment of HI brain injury.

Material and Methods

Animals

All experiments were performed in accordance with Duke University Institutional Animal Care and Use Committee's policies and followed approved protocols. C57BL/6 mice (The Jackson Laboratory) and CX3CR1-GFP^{+}/- mice were maintained in Duke Facilities under direct veterinary supervision. Animals had ad libitum access to food and water in a temperature-controlled room under a 12-hour light: 12-hour dark illumination cycle.

Oxygen-glucose deprivation (OGD) of brain slice cultures

Organotypic forebrain slice cultures were prepared following the method described by Stoppini *et al*.[21] . Briefly, 300µm thick forebrain sagittal slices from postnatal day-2 mouse pups were sectioned. The sections were cultured under controlled atmospheric conditions on top of cell impermeable membranes in contact with culture medium. Slices were exposed to medium without glucose in an oxygen-free gas mixture for one hour, returned to normoxic, glucose replete conditions, and incubated for 72 hours before further analysis.

Treating slice cultures with cells

To test the protective activity of human CB or PB cell populations, 2.5 x 10^4 cells were added directly onto each brain slice immediately after OGD shock. Alternatively, cell populations were added to the tissue culture medium below the membrane supporting slices. Cell death and/or the cellular composition of the slice cultures were compared to control slices not treated with cells 72 hours after OGD treatment.

Evaluation of cell death following OGD

Slices were transferred to medium containing propidium iodide (PI, 2.0 µg/mL, Sigma) and incubated for 30 minutes to stain late apoptotic and necrotic cells, washed thoroughly with PBS, fixed with 4% paraformaldehyde [PFA] containing 4,6-diamidino-2-phenylindole (DAPI). Slides were coded, and percentage of total cells (DAPI staining) that were dead (PI staining) in multiple sequential images of the periventricular region was determined. To minimize regional variation, we kept the region of analysis uniform (periventricular region) between experimental groups. Each slide was analyzed by an investigator blinded to the identity of the experimental material using a Leica SP8 upright confocal microscopy (Leica Microsystems, IL, USA) and ImageJ and Plugin Cell Counter (NIH Image, USA) software.

Immunohistological analysis of cell populations in slice cultures.

Brain slices were fixed in 4% PFA and blocked in phosphate buffered saline (PBS) containing 3% heat-inactivated horse serum, 2% bovine serum albumin (BSA), and 0.25% triton-X-100 overnight. Primary antibody was prepared in 2% BSA, 0.25% triton X-100 in PBS. Slides were incubated in antibody for 24-48 hours and subsequently washed once for 30 minutes and twice for 1 hour in PBS. Secondary antibody was prepared in 2% BSA in PBS. Slides were incubated 24 hours, subsequently washed once 30 minutes and twice for 1 hour and mounted with Vectashield (Vector Labs, CA, USA). Images were analyzed as described for PI staining. All details concerning antibodies are presented in S1 Table.

Sholl Analysis Method for microglial activation

We used CX3CR1-GFP^{+}/- mice pups to set up the slice culture to do Sholl analysis to quantify microglial projections. Unbiased Sholl analysis was done by selecting 3-4 representative

microglial cells in each max projection image using Fiji (ImageJ). Each image was thresholded by eye to convert each 32-bit grayscale image to a compatible 8-bit image with an inverted LUT. The freehand selection tool was utilized to appropriately select the desired microglial cell and clear the outside. The straight-line tool was used to define the largest Sholl radius, beginning in the center of the cell and arbitrarily extending outward. Sholl analysis was performed under the 'most informative' normalized profile, which auto-determines whether to use a semi-log or log-log method of analysis [26]. Area was used as the normalizer in each profile. Parameters were set with a beginning radius of 5 microns, an ending radius of 49 microns, and a step size of 2 microns. The enclosing radius cutoff was set at 1 intersection. Data presented in the associated figure (Fig 2) was deduced at by averaging the number of intersections per step size per group.

Isolation of human umbilical cord and adult peripheral blood mononuclear cells

Freshly collected human umbilical cord blood was provided by the Carolinas Cord Blood Bank at Duke, an FDA licensed public cord blood bank that accepts donations of cord blood collected after birth from the placentas of healthy term newborns after written informed consent from the baby's mother. Also with maternal informed consent, cord blood units not qualifying for banking for transplantation were designated for research and made available for this study. Peripheral blood (PB) was obtained via venipuncture from healthy adult volunteer donors. Procurement of human samples were obtained using protocols approved by the Duke University Institutional Review Board. Mononuclear cells were isolated from CB and PB by density centrifugation using standard Ficoll-Hypaque technique (GE Healthcare) then treated with 0.15M NH_4Cl to lyse residual erythrocytes and washed in phosphate-buffered saline (PBS).

Immunomagnetic cell isolation of various sub-populations of CB and PB experiments

Specific sub-populations were isolated or removed from CB-MNC or PB-MNC by immunomagnetic sorting using EasySep cell kits for human $CD34^+$, $CD3^+$, $CD14^+$ and $CD19^+$ cells (Stemcell Technologies, Vancouver, Canada, Catalog #18096, #18051, #18058 and #18054 respectively) following the manufacturer's directions. Flow-through fractions from positive selection columns were re-run through the columns to increase the purity of targeted populations. A sample of each cell preparation was analyzed by flow cytometry to determine cellular composition [27]. Immuno-magnetically selected specific sub-population of cells with ≥80% purity was used for any experiment. More highly purified populations were obtained by cell sorting as described below for gene expression analysis.

RNA isolation and microarray analysis

RNA isolation and microarray analysis were carried out exactly as described previously using 54,675 probe set Affymetrix GeneChip Human Transcriptome Array 2.0 microarrays and Partek Genomics Suite 6.6 (Partek Inc., St. Louis, MO) software for analysis [27]. S1 Table outlines the experimental methods to prepare cells used for RNA extraction, the number of donors, and the characteristics of the donors used for each chip. Full expression analysis of CB data from Experiment 714 was previously published [27]; comparison of CB to PB-$CD14^+$ cells was not included in that publication. S2 Table provides demographic information on the donors and describes the preparation of $CD14^+$ cells used for the analysis, and numbers we used to designate the experiments in the text.

Western blotting

Western blotting was carried out as previously described [27] using antibodies described in S1 Table.

Statistical analysis:

Data analysis was performed by calculating the mean of the values for each individual group ± standard error of mean and shown, graphically. Statistical analyses were carried out with GraphPad Prism software. All comparisons were performed by one-way analysis of variance (ANOVA) followed by post-hoc analysis with Bonferroni correction. Mean differences were considered significant if $p<0.05$ was computed.

RESULTS

CB-MNC protect organotypic brain slice culture cells from OGD induced damage

Mouse brain organotypic slice cultures were exposed to OGD for 1-hour and returned to the normoxic condition with media containing glucose for the cell treatment. A schematic diagram of the organotypic brain slice culture system is shown in S1A Fig. The extent of damage in the brain slice culture was evaluated by cellular PI uptake after the ischemic insult and following cell treatment. We found a significant number of cells in mouse brain slice cultures became permeable to PI during the three days following OGD shock Fig 1A. Addition of 25,000 CB-MNC to the surface of each OGD-shocked brain slice reduced the number of PI-stained dead cells significantly compared to the OGD-shocked control slices cultured without CB cells. This decrease in the number of dead cells in OGD-shocked cultures protected by CB-MNC approached background cell death in normoxic cultures. Quantitative analysis of PI-positive cells showed that the protective effect of CB-MNC was dose dependent between 2,500 to 25,000 CB-MNC per slice; only 25,000 CB-MNC/slice gave statistically significant ($p<0.01$) protection (Fig 1B). Accordingly, we used this dose of cells for all other subsequent experiments. When we added CSFE-labeled CB-MNC directly onto brain slices, we detected green fluorescent cells on the membrane near to and on the s 72 hours after the cell addition (S1B Fig). Staining with antibody to human nuclear antigen confirmed that these CFSE labeled cells were human cells (S1B Fig).

To determine if paracrine factors released from CB-MNC contribute to their neuroprotective effects on OGD-shocked brain slices, we added CB-MNC to the medium below the membrane instead of directly onto the OGD-shocked slices. This prevented direct contact between CB-MNC and brain cells, but permitted agents secreted by CB-MNC to access to the cells in the

brain slices through the 0.4µm pores. To compensate for possible dilution of protective factors by the large volume the culture medium, we added $1.25x10^5$ cells below the membrane. Adding CB-MNC below the membrane reduced brain cell death (Fig 1C). Thus, neuroprotection by CB-MNC after OGD is mediated at least in part through secreted factors.

To identify what cell-types within CB-MNC mediated neuroprotection following OGD, we tested the ability of CB-MNC depleted of specific cell populations as well as isolating specific populations of cell from CB-MNC in our above organotypic cell death assay. Immunomagnetically enriched $CD14^+$ monocytes from CB were sufficient to protect slices from OGD, and CB-MNC depleted of $CD14^+$ monocytes were no longer able to confer protection (Fig 1 D). Depleting other populations, e.g $CD3^+$ T-lymphocyte or $CD19^+$ B-lymphocytes or $CD34^+$ hematopoietic progenitor cells from CB-MNCs did not block protection.

CB CD14$^+$ monocytes protect neurons and reduce glial activation

CB-$CD14^+$ monocytes preserved neurons and dampened microglial and astrocytic activation following OGD. Cell death following OGD was mirrored by a large decrease in the NeuN-positive neuronal nuclei (Fig 2A and Fig 2B). Astrocytes in the cultures that were treated with OGD became hypertrophic and extended multiple processes taking on a characteristic activated morphology (Fig 2C) [28, 29]. Astrocytes were less activated in CB-$CD14^+$ treated slices than CD14-depleted CB-MNC or untreated OGD slices (Fig 2C). It is well established that microglial change morphology from a highly ramified resting state to a reactive/amoeboid state upon ischemic insult [30]. To visualize the microglial morphological change much easily we initiated the organotypic brain slice cultures using CX3CR1-GFP^+/- mice P2 pups. Sholl analysis of these

morphological changes reflecting microglial activation showed that CB-monocytes prevented microglial proliferation and activation in slices exposed to OGD (Fig 2D–Fig 2F).

PB-MNC or purified PB-CD14$^+$ cells failed to protect from OGD induced tissue damage

Since PB-MNC are plentiful in patients with unresolved HI induced injuries we hypothesized that PB-MNCs would not protect against OGD insult. Unlike CB-MNCs, PB-MNCs, CD14$^+$ depleted PB-MNC, or isolated CD14$^+$-PB monocytes were unable to prevent cell death (Fig 3A) or loss of neurons (Fig 3B), following OGD insult.

The differences in activity between CB-MNC and PB-MNC provided an approach to begin to explore the mechanisms by which CB-MNC protect brain cells from hypoxic injury. We reasoned that transcripts for mechanistically important factors would be over-expressed in CB-MNC relative to PB-MNC. To identify these transcripts, we compared whole transcriptome microarrays analysis of CB- and PB-MNC. As described in the Supporting Information section, in all, we analyzed seven adult PB donors and seven CB donors in two separate experiments (714 and 1213) and found that CB and PB-CD14$^+$ monocytes have unique mRNA expression profiles. A heat map presentation of the data analysis of experiment experiments 1213 (Fig 4A), for example, shows that CB and PB-CD14$^+$ monocytes differentially expressed 1553 transcripts. Of these, 474 probes detected transcripts expressed only in PB-CD14$^+$ monocytes, and another 204 probes detected transcript only expressed in CB-CD14$^+$ monocytes. CB and PB-CD14$^+$ monocytes fall into discrete populations defined by these differentially expressed transcripts. Since CB monocytes protect at least in part through secreted factors, we determined which differentially expressed genes (identified in both experimental analyses) encoded secreted proteins or proteins that directly synthesized secreted products. Seven candidates emerged from

this analysis (Table 1). We next analyzed these seven candidate proteins in cell lysates from CB and PB CD14$^+$ monocytes (Fig 4C). CB monocytes expressed more CHI3L1, INHBA, IL10, MMP9, and TSP1 than PB-CD14$^+$ monocytes. Cystathionine (CTH) and VEGFA were strongly, but not differentially, expressed by both CB- and PB-MNC (data not shown). We also used immunocytochemistry to determine how CHI3L1, MMP9 and TSP1 proteins were expressed within CB and PB-CD14$^+$ monocyte populations. S2 Fig shows that CHI3L1 and TSP1 were more strongly expressed in CB than PB-CD14$^+$ monocytes and that these two proteins were present in virtually all CD14$^+$ monocytes. CB monocytes also expressed more MMP9 than PB monocytes, but in this case, expression was confined to a subpopulation of CD14$^+$ monocytes that was less common in PB monocyte populations.

DISCUSSION

We demonstrated that CB-MNC, specifically the CB-CD14$^+$ cells, protect neurons from death after OGD insult. Depleting CD14$^+$ cells, but not other cell types, abrogated the neuroprotective effects of CB-MNC. Purified CD34$^+$ cells also have neuroprotective activity, but given that depleting CD34$^+$ cells did not alter neuroprotection and that CD14$^+$ cells are 10-50-fold more abundant in CB MNC than CD34$^+$ cells, we attribute the neuroprotective activity of CB-MNC in our assay system to CD14$^+$ cells. Neuroprotection was mediated primarily by soluble factors produced by CD14$^+$ monocytes. This corroborates previous studies demonstrating that infiltrating monocytes sequestered in the brain meninges modulate brain inflammation and promote repair following HI injuries [31, 32]. CB CD14$^+$ monocytes used as a therapeutic agent may have similar effects whether administered alone as a selected subpopulation or as a component present in the total CB-MNC.

Unlike CB monocytes, PB monocytes had little or no impact on glial activation or cell death in the OGD assay. We identified differentially expressed genes enriched in CB monocytes compared to PB monocytes. Based on our transwell experiments and other published data [10, 14] demonstrating that CB-MNC mediated repair of brain tissue through paracrine factors, we focused on finding secretory molecules over expressed in CB monocytes. Proteins encoded by five (*CHI3L1, TSP1, MMP9, IL10*, and *INHBA*) of the seven candidate genes we initially identified were more abundant in homogenates of CB than PB monocytes. TSP1 [33-37], CHI3l1 [38-41]; MMP9 [42-46], IL10 [47], and INHBA [48, 49] can all promote tissue repair, including repair in the brain. TSP1, CHI3l1 and MMP9 showed the largest difference in protein expression, and CB monocytes have more of these three proteins in cytoplasmic granules, presumably secretory granules, than PB monocytes. Thus, CHI3l1, TSP1, and MMP9 may be

particularly important in paracrine mechanisms by which CB monocytes reduce glial activation and protect brain neurons from OGD. Furthermore, correlating the biological and clinical activities with expression of these markers may provide a path to a biologically based potency assay for CB products in brain repair indications.

Though our work suggests that secretory proteins CHI3l1, TSP1, and MMP9 from monocytes might contribute to neuroprotection, other important protective gene products are probably induced by CB monocytes in or near HI-shocked brain tissue. The OGD-shocked brain slice model should be useful in identifying these gene products and elucidating more precisely how CB monocytes intervene in the pathogenic process.

Finally, most preclinical studies and clinical trials involving the use of CB-MNC as therapeutics for HI brain injuries have involved intravenous delivery of cell product. The OGD model in which cells are added directly to brain slices, or in a small amount of medium directly below the slices, may not reflect the dosing or pharmacokinetics associated with intravenous administration. We found a dose dependency over a ten-fold range of CB monocyte concentration in the OGD model even though cells were directly applied to slices. In hematopoietic stem cell transplant patients receiving intravenously injected CB-MNC grafts, most CB cells are removed in the lungs and other organs during first pass circulation. Animal studies have shown that some unidentified CB cells are present near brain lesions for short periods of time following intravenous treatment of acute stroke [50] or neonatal HIE with CB-MNC [51] but the function of these cells is unclear. Some evidence suggests that CB-MNC respond to chemokines by migrating to ischemic brain regions [52-54]. Womble et al. found that the beneficial activity of intravenously injected CB-MNC in a rat stroke model resided in the $CD14^+$ monocyte population. How many CB-MNC or monocytes that reach the brain following

intravenous injection in patients with HI-induced brain injury is unknown. Indeed, some animal studies have suggested that intravenously injected CB-MNC products [55] do not need to reach the brain in order to promote repair of stroke or other HI brain injury. Instead, cell products reaching the lungs or spleen may induce endogenous cells to produce soluble factors or activated cells that go to the brain and mediate repair [56-58]. Future studies investigating the biodistribution of CB monocytes will determine the most effective route and dose for administration.

In summary, monocytes in CB, but not PB, protect brain neurons from death and reduce glial activation following HI insult in an *in vitro* OGD model. Soluble factors released from CB monocytes contribute to this protection. We have identified secreted proteins enriched in CB $CD14^+$ monocytes compared to PB monocytes that may play a role in neuroprotection and repair. This work enables future detailed study of the mechanism of neuroprotection and development of mechanism-based release assays for CB products, and formulation of new strategies for using CB monocytes as therapeutic agents in treatment of HI-induced brain injuries.

ACKNOWLEDGMENTS

The authors are grateful to Susan Buntz for helping with flow-cytometry, the staff at the Carolinas Cord Blood Bank for providing cord blood units, to Dr. Michael Cook at the Duke Cancer Center Flow Cytometry Facility for sorting cells, and to Zhengzheng Wei at the Duke Institute for Genomic Sciences Microarray Core Facility for performing microarray analyses. This work was supported by grants from the Julian Robertson Foundation and the Marcus Foundation.

The authors also wish to acknowledge the friendship and the daily advice on both practical and theoretical matters given freely to them by Dr. Bob Storms during the course of this research. Bob died on May 22, 2017.

DISCLOSURE OF POTENTIAL CONFLICTS OF INTEREST

The authors disclose no conflicts of interest.

REFERENCES

1. Sun, J., et al., *Differences in quality between privately and publicly banked umbilical cord blood units: a pilot study of autologous cord blood infusion in children with acquired neurologic disorders.* Transfusion, 2010. **50**(9): p. 1980-7.
2. Bae, S.H., et al., *The levels of pro-inflammatory factors are significantly decreased in cerebral palsy patients following an allogeneic umbilical cord blood cell transplant.* Int J Stem Cells, 2012. **5**(1): p. 31-8.
3. Sharma, A., et al., *Administration of autologous bone marrow-derived mononuclear cells in children with incurable neurological disorders and injury is safe and improves their quality of life.* Cell Transplant, 2012. **21 Suppl 1**: p. S79-90.
4. Feng, M., et al., *Safety of Allogeneic Umbilical Cord Blood Stem Cells Therapy in Patients with Severe Cerebral Palsy: A Retrospective Study.* Stem Cells Int, 2015. **2015**: p. 325652.
5. Cotten, C.M., et al., *Feasibility of autologous cord blood cells for infants with hypoxic-ischemic encephalopathy.* J Pediatr, 2014. **164**(5): p. 973-979 e1.
6. Cui, X., et al., *Therapeutic benefit of treatment of stroke with simvastatin and human umbilical cord blood cells: neurogenesis, synaptic plasticity, and axon growth.* Cell Transplant, 2012. **21**(5): p. 845-56.
7. Sun, J.M., et al., *Effect of Autologous Cord Blood Infusion on Motor Function and Brain Connectivity in Young Children with Cerebral Palsy: A Randomized, Placebo-Controlled Trial.* Stem Cells Transl Med, 2017.
8. Bennet, L., et al., *Cell therapy for neonatal hypoxia-ischemia and cerebral palsy.* Ann Neurol, 2012. **71**(5): p. 589-600.
9. Yu, G., et al., *Systemic delivery of umbilical cord blood cells for stroke therapy: a review.* Restor Neurol Neurosci, 2009. **27**(1): p. 41-54.
10. Tsuji, M., et al., *Effects of intravenous administration of umbilical cord blood CD34(+) cells in a mouse model of neonatal stroke.* Neuroscience, 2014. **263**: p. 148-58.
11. Iskander, A., et al., *Intravenous administration of human umbilical cord blood-derived AC133+ endothelial progenitor cells in rat stroke model reduces infarct volume: magnetic resonance imaging and histological findings.* Stem Cells Transl Med, 2013. **2**(9): p. 703-14.
12. Shahaduzzaman, M., et al., *A single administration of human umbilical cord blood T cells produces long-lasting effects in the aging hippocampus.* Age (Dordr), 2013. **35**(6): p. 2071-87.
13. Womble, T.A., et al., *Monocytes are essential for the neuroprotective effect of human cord blood cells following middle cerebral artery occlusion in rat.* Mol Cell Neurosci, 2014. **59**: p. 76-84.
14. Boltze, J., et al., *Assessment of neuroprotective effects of human umbilical cord blood mononuclear cell subpopulations in vitro and in vivo.* Cell Transplant, 2012. **21**(4): p. 723-37.
15. Hau, S., et al., *Evidence for neuroprotective properties of human umbilical cord blood cells after neuronal hypoxia in vitro.* BMC Neurosci, 2008. **9**: p. 30.

16. Reich, D.M., et al., *Neuronal hypoxia in vitro: investigation of therapeutic principles of HUCB-MNC and CD133+ stem cells.* BMC Neurosci, 2008. **9**: p. 91.
17. McDonald, C.A., et al., *Effects of umbilical cord blood cells, and subtypes, to reduce neuroinflammation following perinatal hypoxic-ischemic brain injury.* J Neuroinflammation, 2018. **15**(1): p. 47.
18. Jiang, L., et al., *The effect of human umbilical cord blood cells on survival and cytokine production by post-ischemic astrocytes in vitro.* Stem Cell Rev, 2010. **6**(4): p. 523-31.
19. Hall, A.A., et al., *Human umbilical cord blood cells directly suppress ischemic oligodendrocyte cell death.* J Neurosci Res, 2009. **87**(2): p. 333-41.
20. Rowe, D.D., et al., *Cord blood administration induces oligodendrocyte survival through alterations in gene expression.* Brain Res, 2010. **1366**: p. 172-88.
21. Stoppini, L., P.A. Buchs, and D. Muller, *A simple method for organotypic cultures of nervous tissue.* J Neurosci Methods, 1991. **37**(2): p. 173-82.
22. Sundstrom, L., et al., *Organotypic cultures as tools for functional screening in the CNS.* Drug Discov Today, 2005. **10**(14): p. 993-1000.
23. Hall, A.A., et al., *Delayed treatments for stroke influence neuronal death in rat organotypic slice cultures subjected to oxygen glucose deprivation.* Neuroscience, 2009. **164**(2): p. 470-7.
24. Noraberg, J., et al., *Organotypic hippocampal slice cultures for studies of brain damage, neuroprotection and neurorepair.* Curr Drug Targets CNS Neurol Disord, 2005. **4**(4): p. 435-52.
25. Daviaud, N., et al., *Organotypic cultures as tools for optimizing central nervous system cell therapies.* Exp Neurol, 2013. **248**: p. 429-40.
26. Ferreira, T.A., et al., *Neuronal morphometry directly from bitmap images.* Nat Methods, 2014. **11**(10): p. 982-4.
27. Saha, A., et al., *A cord blood monocyte-derived cell therapy product accelerates brain remyelination.* JCI Insight, 2016. **1**(13): p. e86667.
28. Pekny, M., U. Wilhelmsson, and M. Pekna, *The dual role of astrocyte activation and reactive gliosis.* Neurosci Lett, 2014. **565**: p. 30-8.
29. Anderson, M.A., Y. Ao, and M.V. Sofroniew, *Heterogeneity of reactive astrocytes.* Neurosci Lett, 2014. **565**: p. 23-9.
30. Karperien, A., H. Ahammer, and H.F. Jelinek, *Quantitating the subtleties of microglial morphology with fractal analysis.* Front Cell Neurosci, 2013. **7**: p. 3.
31. Lampron, A., P.M. Pimentel-Coelho, and S. Rivest, *Migration of bone marrow-derived cells into the central nervous system in models of neurodegeneration.* J Comp Neurol, 2013. **521**(17): p. 3863-76.
32. Herz, J., et al., *Myeloid Cells in the Central Nervous System.* Immunity, 2017. **46**(6): p. 943-956.
33. Risher, W.C. and C. Eroglu, *Thrombospondins as key regulators of synaptogenesis in the central nervous system.* Matrix Biol, 2012. **31**(3): p. 170-7.
34. Cheng, C., et al., *Thrombospondin-1 Gene Deficiency Worsens the Neurological Outcomes of Traumatic Brain Injury in Mice.* Int J Med Sci, 2017. **14**(10): p. 927-936.

35. Jayakumar, A.R., et al., *Decreased astrocytic thrombospondin-1 secretion after chronic ammonia treatment reduces the level of synaptic proteins: in vitro and in vivo studies.* J Neurochem, 2014. **131**(3): p. 333-47.
36. Sallon, C., et al., *Thrombospondin-1 (TSP-1), a new bone morphogenetic protein-2 and -4 (BMP-2/4) antagonist identified in pituitary cells.* J Biol Chem, 2017. **292**(37): p. 15352-15368.
37. Son, S.M., et al., *Thrombospondin-1 prevents amyloid beta-mediated synaptic pathology in Alzheimer's disease.* Neurobiol Aging, 2015. **36**(12): p. 3214-3227.
38. Lee, C.G., et al., *YKL-40, a chitinase-like protein at the intersection of inflammation and remodeling.* Am J Respir Crit Care Med, 2012. **185**(7): p. 692-4.
39. Wiley, C.A., et al., *Role for mammalian chitinase 3-like protein 1 in traumatic brain injury.* Neuropathology, 2015. **35**(2): p. 95-106.
40. Bonneh-Barkay, D., et al., *In vivo CHI3L1 (YKL-40) expression in astrocytes in acute and chronic neurological diseases.* J Neuroinflammation, 2010. **7**: p. 34.
41. Jingjing, Z., et al., *MicroRNA-24 Modulates Staphylococcus aureus-Induced Macrophage Polarization by Suppressing CHI3L1.* Inflammation, 2017. **40**(3): p. 995-1005.
42. Singh, D., et al., *Multifaceted role of matrix metalloproteinases (MMPs).* Front Mol Biosci, 2015. **2**: p. 19.
43. Ethell, I.M. and D.W. Ethell, *Matrix metalloproteinases in brain development and remodeling: synaptic functions and targets.* J Neurosci Res, 2007. **85**(13): p. 2813-23.
44. Luo, J., *The role of matrix metalloproteinases in the morphogenesis of the cerebellar cortex.* Cerebellum, 2005. **4**(4): p. 239-45.
45. Dziembowska, M. and J. Wlodarczyk, *MMP9: a novel function in synaptic plasticity.* Int J Biochem Cell Biol, 2012. **44**(5): p. 709-13.
46. Kelly, E.A., et al., *Proteolytic regulation of synaptic plasticity in the mouse primary visual cortex: analysis of matrix metalloproteinase 9 deficient mice.* Front Cell Neurosci, 2015. **9**: p. 369.
47. Norden, D.M., et al., *TGFbeta produced by IL-10 redirected astrocytes attenuates microglial activation.* Glia, 2014. **62**(6): p. 881-95.
48. Brackmann, F.A., C. Alzheimer, and R. Trollmann, *Activin A in perinatal brain injury.* Neuropediatrics, 2015. **46**(2): p. 82-7.
49. Wu, D.D., et al., *Expression of the activin axis and neuronal rescue effects of recombinant activin A following hypoxic-ischemic brain injury in the infant rat.* Brain Res, 1999. **835**(2): p. 369-78.
50. Vendrame, M., et al., *Infusion of human umbilical cord blood cells in a rat model of stroke dose-dependently rescues behavioral deficits and reduces infarct volume.* Stroke, 2004. **35**(10): p. 2390-5.
51. Drobyshevsky, A., et al., *Human Umbilical Cord Blood Cells Ameliorate Motor Deficits in Rabbits in a Cerebral Palsy Model.* Dev Neurosci, 2015. **37**(4-5): p. 349-62.
52. Newman, M.B., et al., *Stroke-induced migration of human umbilical cord blood cells: time course and cytokines.* Stem Cells Dev, 2005. **14**(5): p. 576-86.
53. Jiang, L., et al., *MIP-1alpha and MCP-1 Induce Migration of Human Umbilical Cord Blood Cells in Models of Stroke.* Curr Neurovasc Res, 2008. **5**(2): p. 118-24.

54. Rosenkranz, K., et al., *The chemokine SDF-1/CXCL12 contributes to the 'homing' of umbilical cord blood cells to a hypoxic-ischemic lesion in the rat brain.* J Neurosci Res, 2010. **88**(6): p. 1223-33.
55. Borlongan, C.V., et al., *Central nervous system entry of peripherally injected umbilical cord blood cells is not required for neuroprotection in stroke.* Stroke, 2004. **35**(10): p. 2385-9.
56. Vendrame, M., et al., *Cord blood rescues stroke-induced changes in splenocyte phenotype and function.* Exp Neurol, 2006. **199**(1): p. 191-200.
57. Ajmo, C.T., Jr., et al., *The spleen contributes to stroke-induced neurodegeneration.* J Neurosci Res, 2008. **86**(10): p. 2227-34.
58. Seifert, H.A., et al., *The spleen contributes to stroke induced neurodegeneration through interferon gamma signaling.* Metab Brain Dis, 2012. **27**(2): p. 131-41.

FIGURE LEGENDS

Fig 1: Human cord blood mononuclear cells reduce death of mouse forebrain cells following OGD shock. A) Left panel shows slice cultures not exposed to OGD. Slices in other panels were exposed to OGD for one hour, returned to normoxic, glucose replete conditions, and then cultured for 72 hours after which cell viability was assayed by staining with DAPI (blue) and PI (red). Middle panel shows slices cultured without added CB cells. Right panel shows slices cultured with 25,000 CB-MNC added directly onto slice at the end of OGD. B) Protection of brain cells following OGD depends on dose of CB-MNC added to slices. PI-stained cells were counted in contiguous 10X high power fields in the periventricular region. Bar graphs show mean $^{+}$/- SE of PI-stained cells per 10X high-power filed. Only the 25,000 cell dose group showed protection (n=-3, one way ANOVA, * $p \leq 0.001$). C) Paracrine factors from CB-MNC protect brain slice cultures after OGD shock. CB MNC were added either onto slice (light blue bar, $2.5x10^4$ cells) or in medium below membrane (grey bar, $1.25x10^5$ cells; n=3, one way ANOVA, * $p<0.01$). D) OGD-shocked slices were co-cultured with CB-MNC that had been immunomagnetically depleted of the specific subpopulations or were co-cultured with immunomagnetically selected subpopulations expressing the surface antigen shown. First column on the left shows normoxic controls. All other data from OGD shocked slices (one-way ANOVA; *$p<0.001$).

Fig 2: CB $CD14^{+}$ monocytes protect neurons and reduce glial activation following OGD shock. (A) Confocal images (40x) of antibody stained neurons (green, anti-NeuN) in the periventricular region of control and cell treated brain slice cultures co-cultured three days with various CB cell populations following OGD shock. Top left panel shows control slices not exposed to OGD and

cultured without human cells. All other panels show slices exposed to OGD prior to addition of human cells. Top right panel shows slices co-cultured with selected CB-CD14$^+$ monocytes; and bottom right panel, with CB MNC depleted of CD14$^+$ monocytes. (B) The average number of NeuN$^+$ neurons in 40x high-powered fields (HPF) located along the periventricular region was determined. Values shown are means $^+$/- standard deviation. N=3 slices under each condition. Statistically significant differences ($p<0.01$) compared to the OGD control are indicated by asterisks. (C) Confocal images (40x) of antibody stained astrocytes [magenta, anti- GFAP] in the periventricular region of control and cell treated brain slice cultures co-cultured three days with various CB cell populations following OGD shock. Top row shows control slices not exposed to OGD and cultured without human cells. All other rows show slices exposed to OGD prior to addition of CB cells. Third row shows slices co-cultured with CB-CD14$^+$ monocytes; fourth row, with CB MNC depleted of CD14$^+$ monocytes. (D) Representative confocal images of microglial cells in CX3CR1-GFP$^+$/- mouse brain slice cultures and numbers are shown. (E) Sholl profiles of microglial cells in brain slices of normoxic, OGD-shocked and OGD-shocked treated with CBCD14$^+$ cells. Intersections were counted at 2µm intervals from the soma center to a radius of 5 µm to 50 µm. Curves represent mean intersection values ±SEM. (F) Number of microglia in control and OGD-treated brain slice cultures with and without added **CB** CD14$^+$ cells.

Fig 3: CD14$^+$ CB, but not PB, monocytes protect neurons following OGD shock. (A) CB-MNC, PB-MNC, CD14$^+$ or CD14 depleted PB cells (25,000cells/slice) were added directly onto OGD shocked brain slice cultures as indicated, and PI-positive cells dead were quantified and graphically represented. Statistically significant differences determined by one-way ANOVA ($p<0.001$) compared to the OGD control are indicated by asterisks. (B) Confocal images (40x) of

antibody stained neurons [green, anti-NeuN] of control and cell treated brain slice cultures co-cultured three days with various PB cell populations following OGD shock. Top left panel shows control slices not exposed to OGD and cultured without human cells. All other panels show slices exposed to OGD prior to addition of human cells. Top right panel shows slices co-cultured with PB-CD14$^+$ monocytes; bottom right panel, with PB MNC depleted of CD14$^+$ monocytes. In the right panel bar-graph plot is shown, the average number of NeuN$^+$ neurons, within sequential 40x high-powered fields located along the periventricular region was determined. Values shown are means $^+$/- standard deviation. n=3 slices under each condition. Statistically significant differences ($p<0.01$) compared to the OGD control are indicated by asterisks.

Fig 4. Identification of secretory proteins expressed by CB CD14$^+$ cells that may mediated protections against OGD. (A) Comparative whole transcriptome analysis of CB-CD14$^+$ and PB-CD14$^+$ cells. Heat maps from Experiment 1213 showing differentially expressed probes in CB (CB-CD14$^+$) and PB (PB-CD14$^+$) cells. Up and downregulated genes are displayed in red and blue, respectively. RMA analysis detected significantly ($p<0.05$) different expression (at least two-fold) of probe sets corresponding to 1553 genes. (B) Gene expression comparisons between CB-CD14$^+$ and PB-CD14$^+$ cells by Venn diagram. Genes in overlapping sets show the differential expression in two or three comparison pairs. (C) Protein expression analysis of CB-CD14$^+$ and PB-CD14$^+$ cells. a) Lane 1-3, represent three different samples (n=3) of CB-CD14$^+$ cells and Lane 4-6 represent, three different samples (n=3) of PB-CD14$^+$ cells. The results confirmed enrichment of CH3L1, INHBA, IL-10, matrix metalloproteinase-9 (MMP9) and TSP1 in CB-CD14$^+$ relative to PB-CD14$^+$ monocyte homogenates. GAPDH was used as loading

control. Quantitative expression of each proteins is shown in the table. Statistical significance ($p < 0.05$) is shown by asterisks. b)

TABLES

Table 1. Seven candidate genes encoding secreted factors over-expressed by CB compared to PB-CD14$^+$ monocytes. All probes sets detecting each candidate genes in both microarrays are shown. Cord and peripheral blood donors are described in S1 Table. See text for screen used to identify candidates. P values are derived from RMAD analysis. Notes show MS5 analysis and indicate whether transcripts were detected exclusively in CB [CB only] or in both CB and PB-CD14$^+$ cells [CB>PB].

			Chip Experiment 1213 (n=4)			Chip Experiment 714 (n=3)		
Gene Symbol	Gene Title	Probe set	p-value	Fold-difference	Note	p-value	Fold-difference	Note
CTH	cystathionase	217127_at	5.70E-04	41.9	CB only	1.18E-08	105.1	CB>PB
		206085_s_at	3.44E-03	14.3	CB only	8.14E-08	26.0	CB only
CHI3L1	chitinase 3-like 1	209395_at	1.33E-02	12.6	CB only	4.99E-02	5.0	CB only
		209396_s_at	1.83E-02	10.6	CB only	1.75E-01	2.8	CB=PB
THBS1	thrombospondin 1	215775_at	6.59E-03	3.1	CB>PB	4.71E-03	2.6	CB>PB
		201107_s_at	1.74E-02	3.5	CB>PB	5.84E-04	3.7	CB only
		201109_s_at	1.19E-04	32.1	CB>PB	5.56E-02	9.3	CB>PB
		201108_s_at	7.37E-04	20.5	CB only	8.98E-03	8.4	CB>PB
		201110_s_at	3.78E-05	22.2	CB>PB	1.98E-01	4.3	CB>PB
		235086_at	2.88E-04	35.0	CB>PB	1.78E-02	8.4	CB > PB
		239336_at	2.24E-03	8.8	CB only	4.42E-03	5.5	CB only
MMP9	matrix metallopeptidase 9	203936_s_at	1.18E-03	13.8	CB>PB	1.17E-02	5.4	CB>PB
IL10	interleukin 10	207433_at	1.51E-02	2.5	CB>PB	3.44E-03	2.8	CB>PB
VEGF-A	vascular endothelial growth factor -A	210512_s_at	1.18E-03	3.6	CB>PB	1.91E-01	2.0	CB=PB
		212171_x_at	2.77E-04	4.4	CB>PB	3.38E-02	2.2	CB>PB
		210513_s_at	2.09E-03	4.1	CB>PB	4.97E-02	1.9	CB=PB
		211527_x_at	1.35E-03	5.1	CB>PB	5.31E-02	2.9	CB > PB
INHBA	inhibin, beta A	227140_at	6.07E-03	10.5	CB only	4.36E-02	14.3	CB>PB
		210511_s_at	2.28E-02	2.3	CB>PB	6.75E-02	3.9	CB>PB
		204926_at	not detected			not detected		

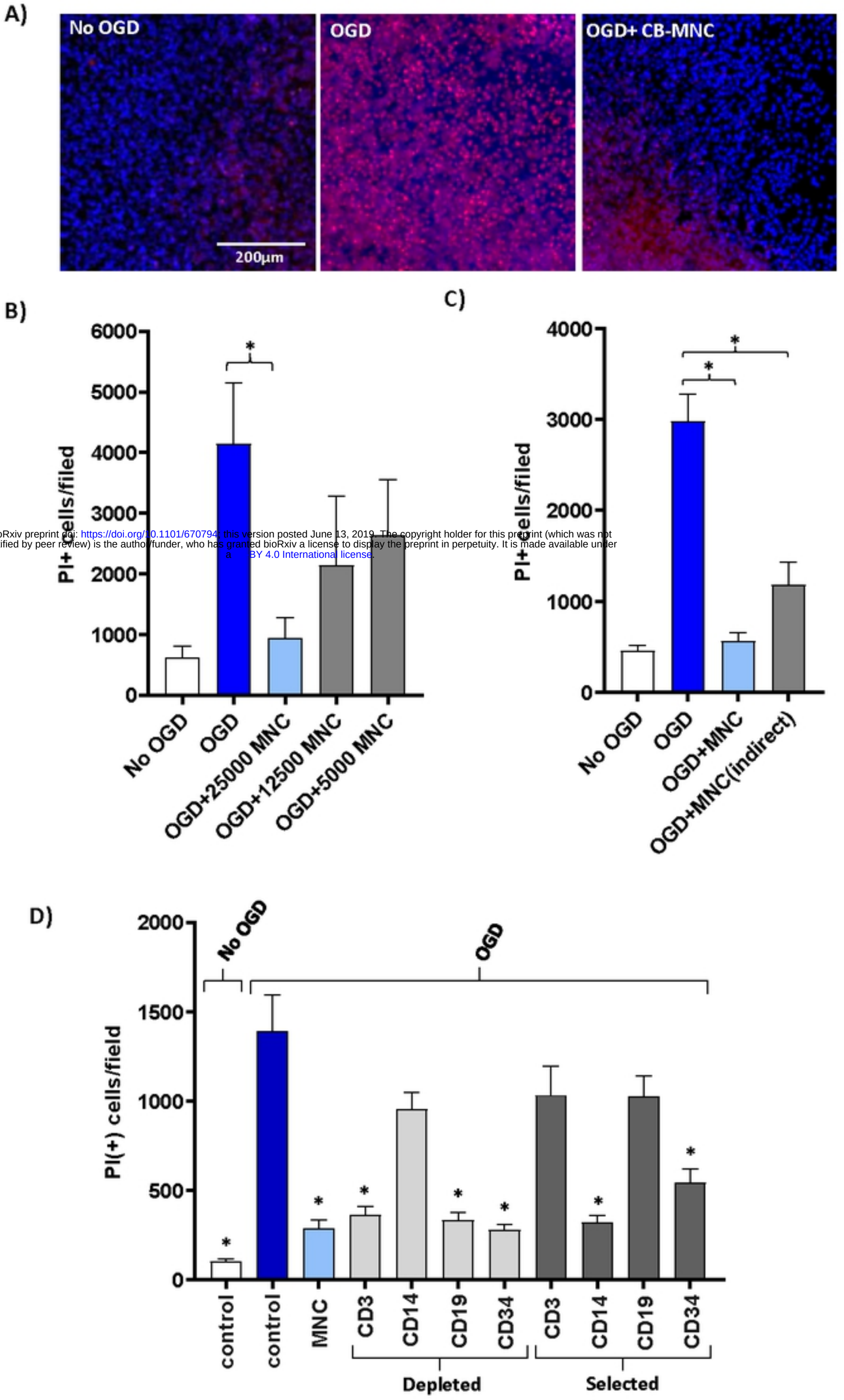

Figure 1

Fig 1

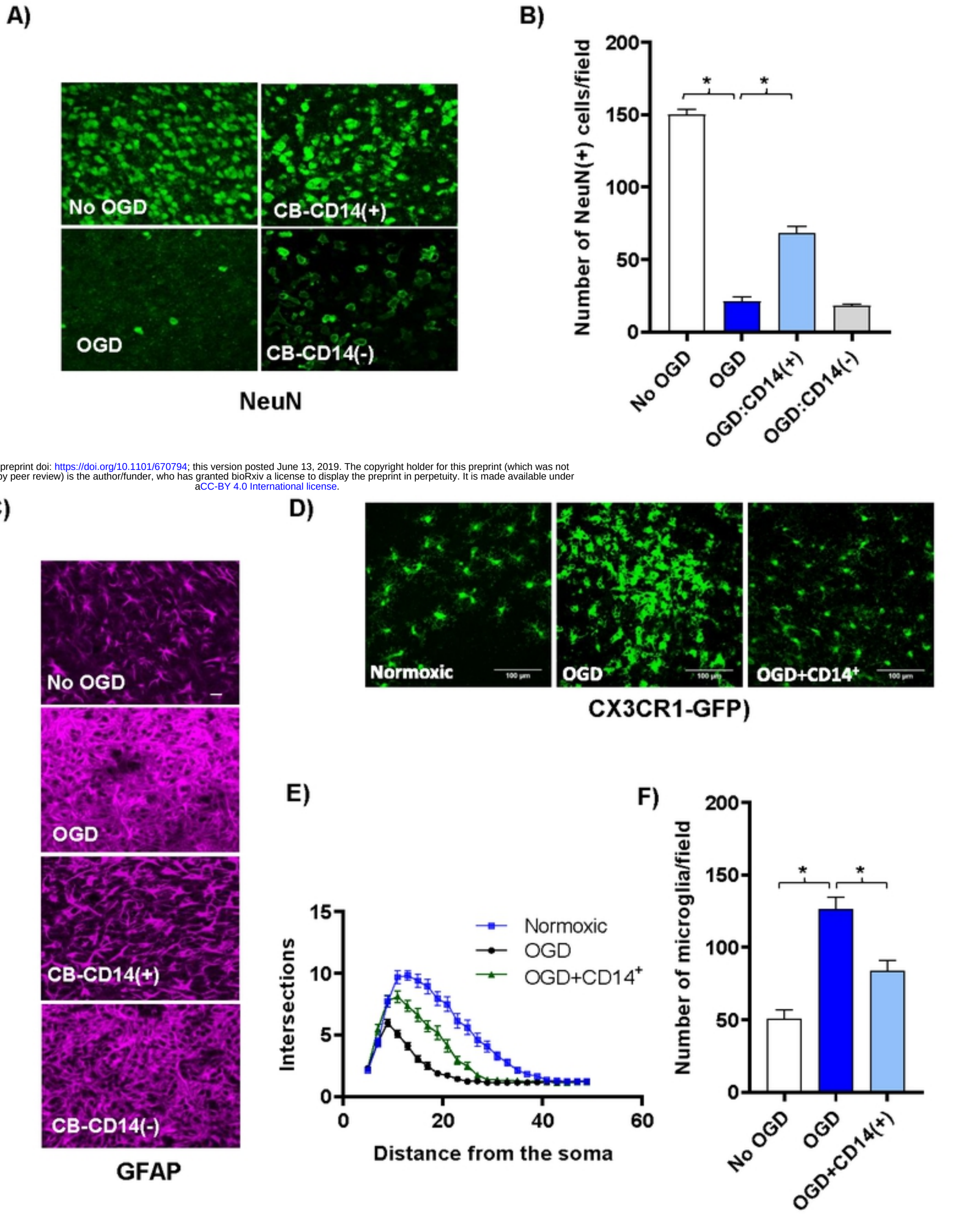

Figure 2

Fig 2

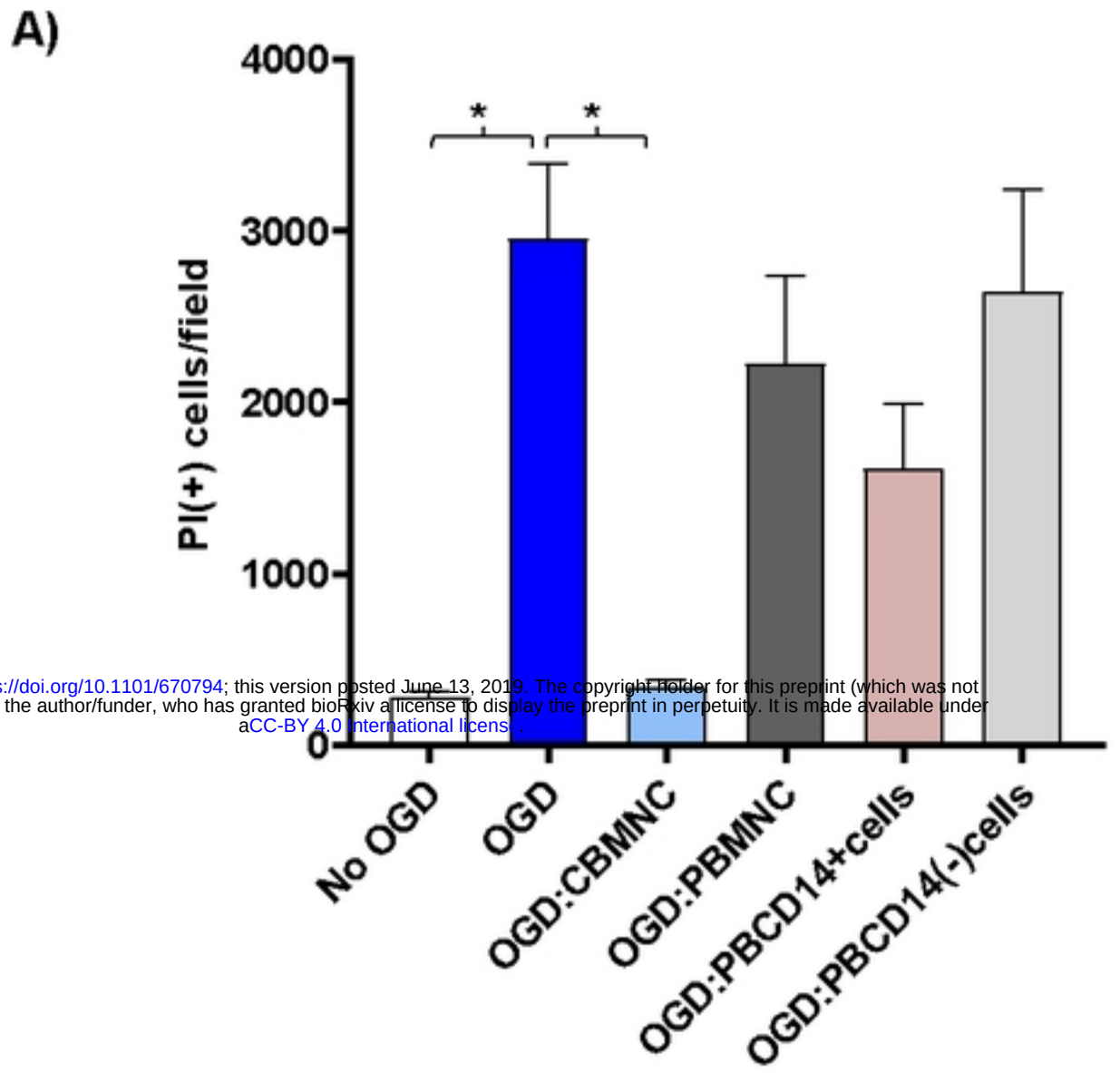

Figure 3

Fig 3

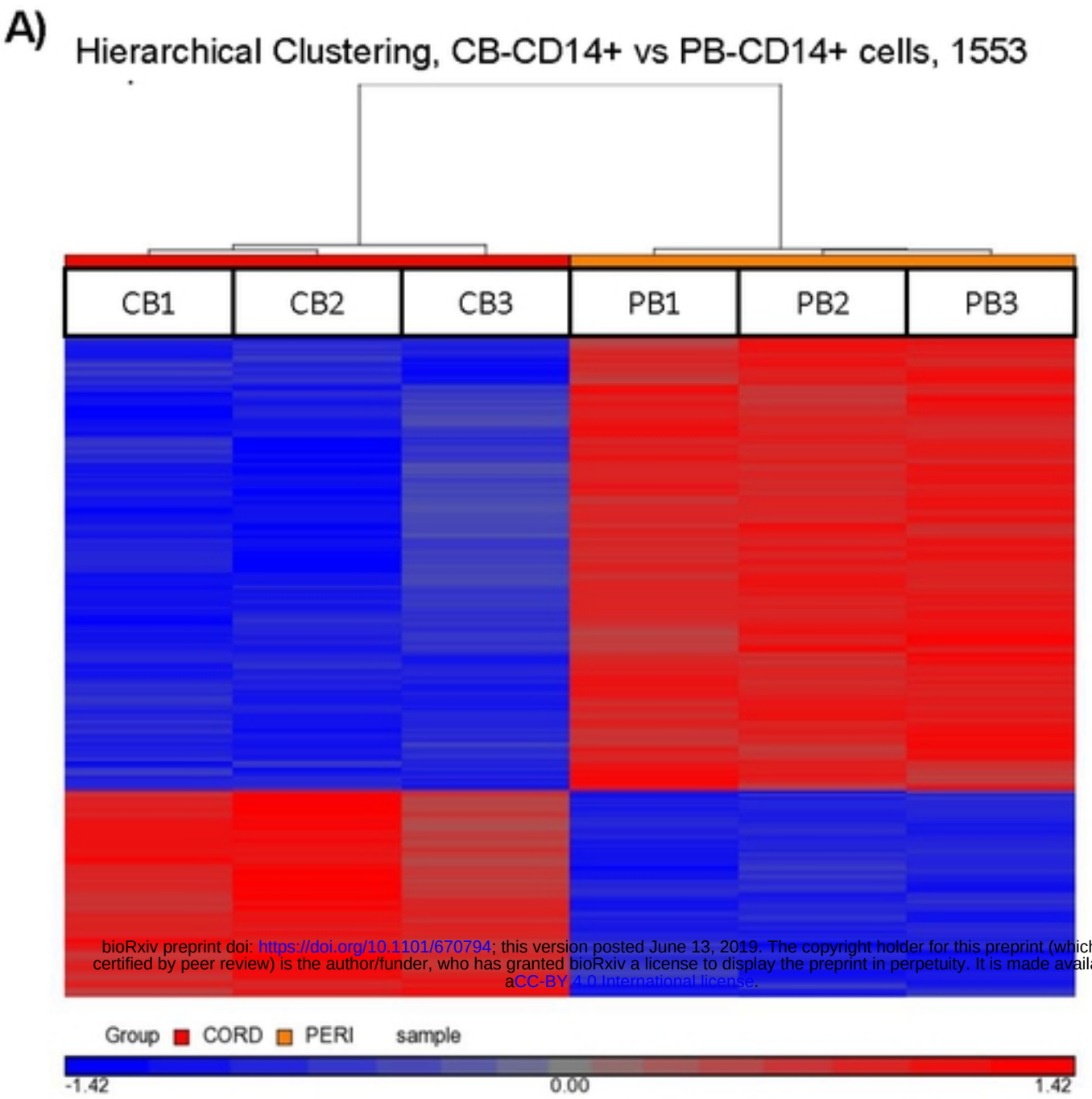

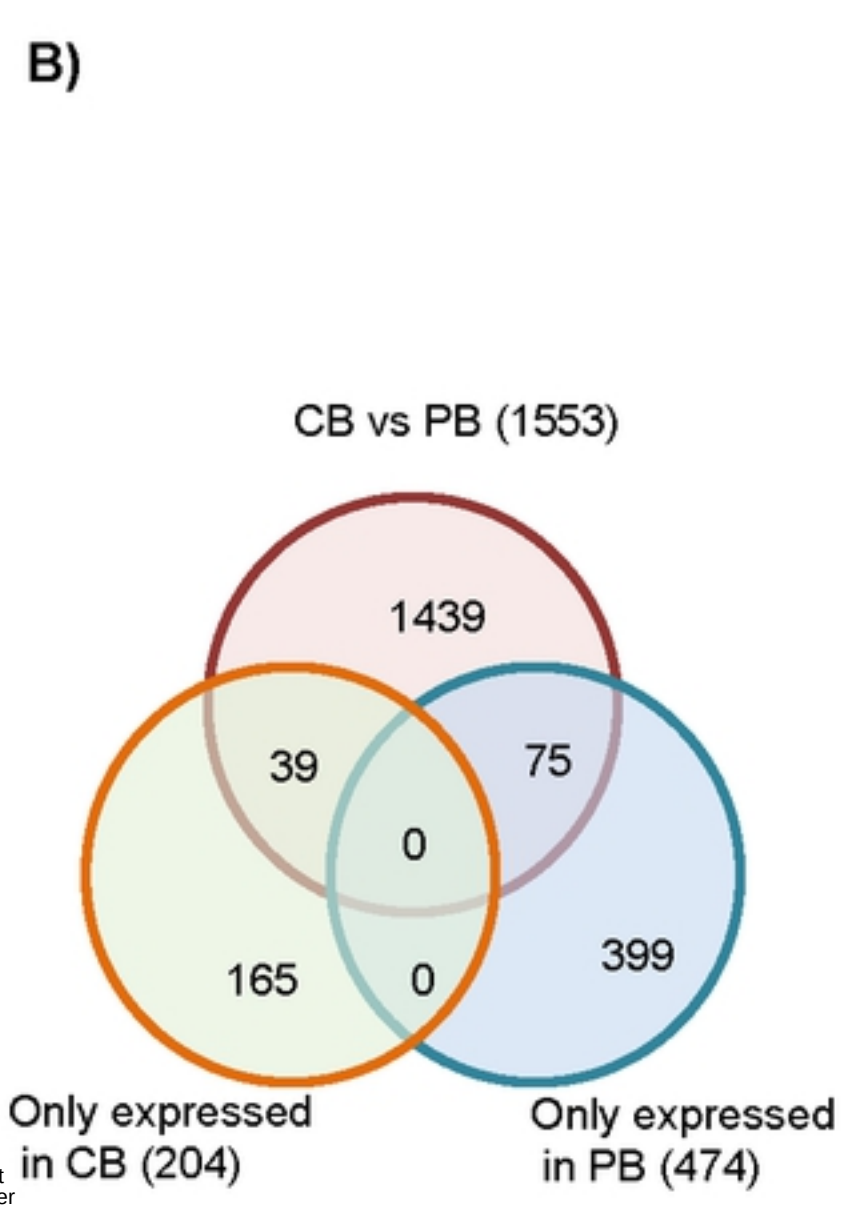

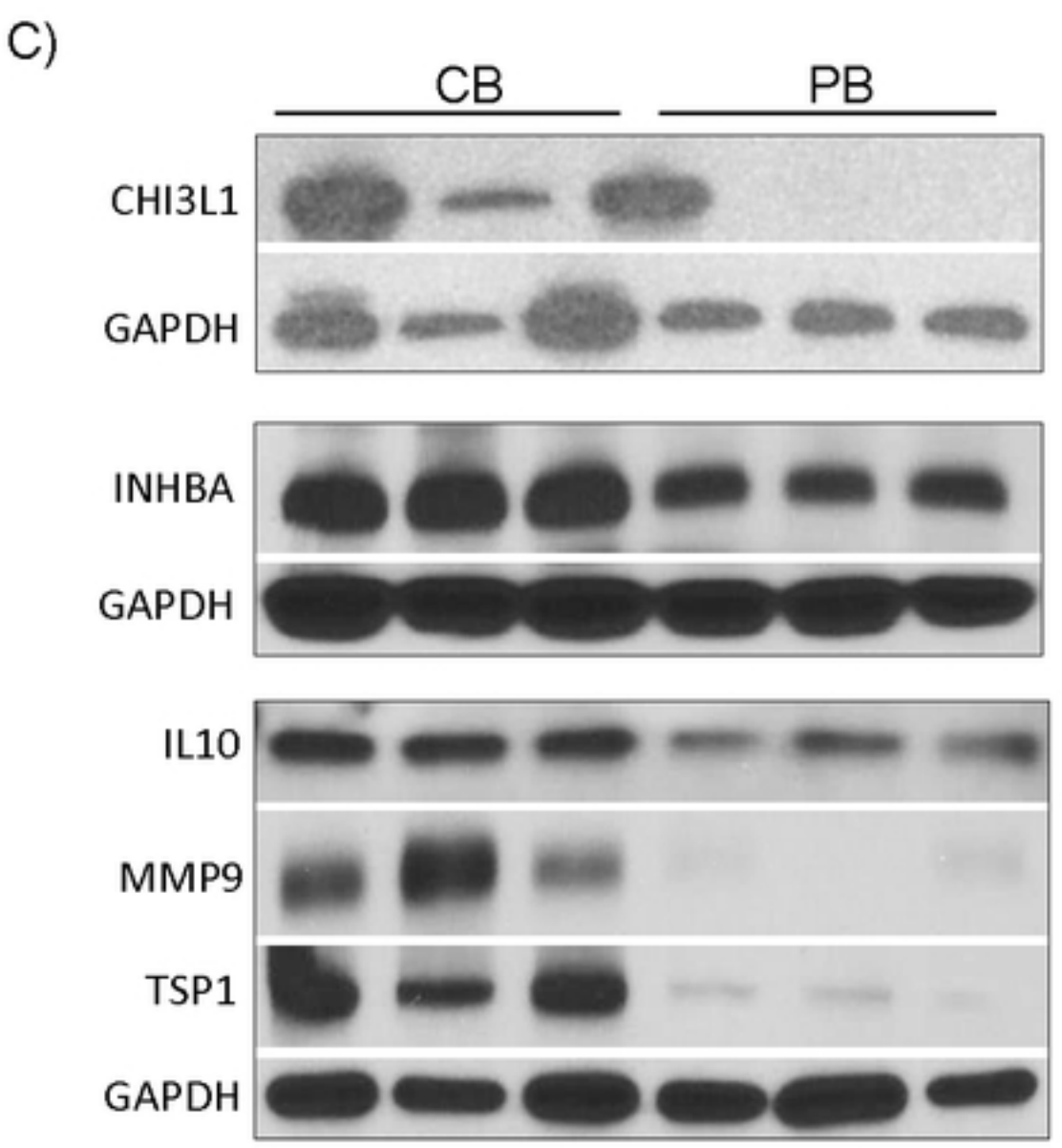

Table: Relative protein expression normalized to GAPDH

	CHI3L1	INHBA	IL10	MMP9	TSP1
CB-CD14+	5.69	1.84	1.41	4.25	8.13
PB-CD14+	1	1	1	1	1
pValue	*	*	*	*	*

Figure 4

Fig 4